

pubs.acs.org/JPCL Letter

Temperature-Dependent Spin-Driven Dimerization Determines the Ultrafast Dynamics of a Copper(II)-Bound Tripyrrindione Radical

Anshu Kumar, Benjamin Thompson, Ritika Gautam, Elisa Tomat, and Vanessa Huxter*



Cite This: J. Phys. Chem. Lett. 2023, 14, 11268–11273



Read Online

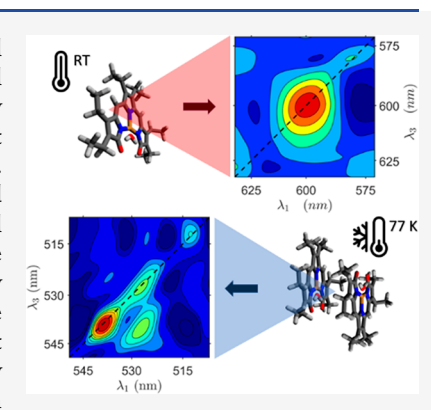
ACCESS I

III Metrics & More

Article Recommendations

Supporting Information

ABSTRACT: Radicals and other open-shell molecules play a central role in chemical transformations and redox chemistry. While radicals are often highly reactive, stable radical systems are desirable for a range of potential applications, ranging from materials chemistry and catalysis to spintronics and quantum information. Here we investigate the ultrafast properties of a stable radical system with temperature-dependent spin-tunable properties. This radical complex, Cu(II) hexaethyl tripyrrin-1,14-dione, accommodates unpaired electrons localized on both the copper metal center and the tripyrrolic ligand. The unusual combination of two unpaired electrons and high stability in this radical molecule enable switchable temperature-dependent spin coupling. Two-dimensional electronic spectroscopy measurements of Cu(II) hexaethyl tripyrrin-1,14-dione were collected at room temperature and at 77 K. At room temperature, the molecules are present as monomers and have short picosecond lifetimes. At 77 K, the molecules are present in a dimer form mediated by ferromagnetic and antiferromagnetic coupling. This reversible spin-driven dimerization changes the optical properties of the system, generating long-lived excitonic states.



Metal-bound radical systems are of particular interest for their ability to perform electron transfer and enable chemical reactivity. They participate in a wide range of biological processes, including photosynthesis and enzyme catalysis. For example, the oxidation of alcohols by the fungal enzyme galactose oxidase is facilitated by a combination of a copper metal center and a tyrosine radical cofactor. In natural light harvesting, the oxidation of chlorophyll, a macrocyclic chlorin with a phytyl chain bound to a magnesium metal center, generates a cationic radical that enables water splitting. Complexes consisting of a transition metal center bound to organic ligands have been widely used in photoredox catalysis. Following optical excitation, these systems can form highly reactive radicals that permit challenging chemical transformations without the use of harsh conditions.

In this paper we present the ultrafast dynamics of a stable neutral radical complex featuring both a ligand-based and a metal-based unpaired spin: a hexaethyl tripyrrin-1,14-dione radical bound to a Cu(II) center (i.e., $[Cu(TD1^{\bullet})(H_2O)]$, abbreviated TD1-Cu). This configuration is unusual and allows for the direct investigation of novel spin-mediated dynamics and interactions. The square-planar TD1-Cu complex, shown in Figure 1a, features a monodentate aqua ligand and a tridentate tripyrrindione, with an electron-rich planar π system capable of reversible one-electron oxidation and reduction chemistry that is of interest for catalytic and redox sensing applications. The neutral radical TD1-Cu complex has one unpaired electron formally in the π system of the tripyrrindione ligand and a second unpaired electron associated with the d9 copper center. These unpaired spins are

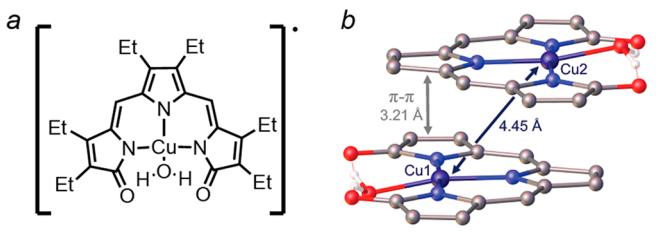


Figure 1. (a) Structure of TD1–Cu (i.e., $[Cu(TD1^{\bullet})(H_2O)])$ and (b) selected metrics of a representative π dimer observed in the crystal structure (CCDC 1496214). Carbon-bound hydrogen atoms and ethyl substituents are omitted for clarity.

in near-orthogonal orbitals, resulting in an overall triplet ground state.¹¹

Recently, our group reported the ultrafast dynamics of TD1–Cu at room temperature by using transient absorption spectroscopy. These studies showed that the lifetime of the excited state of the monomer biradical form of TD1–Cu was sub-20 ps. ¹⁴ At low temperature, metal-bound tripyrrindione radicals reversibly form π stacked dimers, as shown in Figure 1b, mediated by multicenter interactions (also described as

Received: September 28, 2023 Revised: November 22, 2023 Accepted: December 6, 2023 Published: December 7, 2023





pancake bonding^{15,16}) and antiferromagnetic coupling between the unpaired electrons on the ligands. ^{11,17,18} Here we use time-resolved ultrafast spectroscopy to show that the formation of a spin-coupled dimer changes the electronic dynamics. In this paper, we use temperature-dependent two-dimensional electronic spectroscopy (2DES) to observe ultrafast dynamics of TD1–Cu in its monomeric and dimeric forms. These measurements show that TD1–Cu forms excitonic dimers with long-lived excited states at low temperatures compared with the short excited-state lifetime of the room temperature radical monomer.

Figure 2 shows the temperature-dependent absorption spectrum of TD1–Cu in a methylcyclohexane:toluene mixture

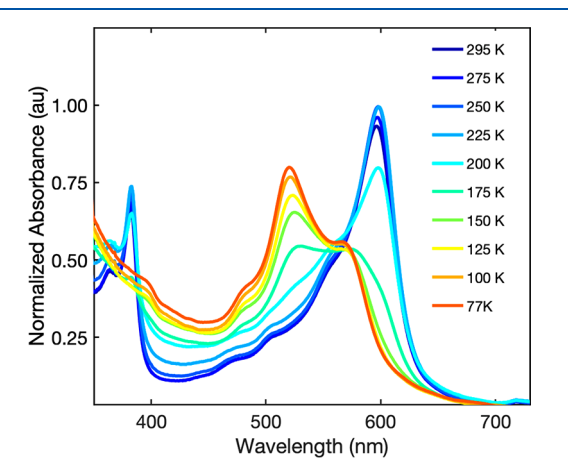


Figure 2. Steady-state absorption of TD1–Cu in a 6:1~v/v methylcyclohexane—toluene mixture, illustrating the temperature-dependent changes from 295 to 77~K.

(6:1 volume ratio) from 295 to 77 K. The steady-state absorption spectra were collected using an Agilent Cary 100 spectrophotometer. No fluorescence was observed for TD1–Cu in the monomer or the dimer form. In our previous work on TD1–Cu, we did not observe any fluorescence at room temperature for either the neutral radical or the oxidized species. ¹⁴ The lack of fluorescence in TD1–Cu is unsurprising

due to the existence of low-lying states that allow relaxation via radiationless transitions (energy gap law). These low-lying states with very small oscillator strengths are characteristic of ligand-based radicals of oligopyrrole complexes and appear in the near-IR region (see Figure S1 in the Supporting Information).

The 295 K absorption spectrum displays a prominent band in the visible region at 600 nm. These transitions originate from π to π^* transitions¹⁴ localized on the tripyrrindione ligand. As the temperature is lowered, the primary absorption peak in the visible shifts from 600 to 521 nm. This change in the absorption spectrum is associated with the formation of a dimer at low temperatures enabled in part by interactions between unpaired electrons. In the monomer, the unpaired electron on the metal center is localized in the $d_{x^2-y^2}$ orbital, which is near orthogonal to the ligand's π orbitals that accommodate the other unpaired electron, 11,14 stabilizing the triplet ground state. Upon lowering the temperature, TD1-Cu undergoes a reversible dimerization process facilitated by antiferromagnetic coupling between the electrons localized on the ligand as well as ferromagnetic interactions between the electrons localized on the Cu(II) metal centers. 11 The presence of an isosbestic point implies the existence of two interconverting equilibrium populations and is representative of the conversion of the monomer to the dimer. The peaks in the near-IR region (Figure S1) also shift and display isosbestic points, consistent with dimerization involving a change in the local environment of the ligand-based electron. Upon freezing into a glass, the scatter from the sample increases slightly, leading to a small amount of uncertainty in the isosbestic point.

The temperature-dependent absorption data was used to determine thermodynamic parameters for the dimerization process in the methylcyclohexane—toluene mixture. Assuming that the monomer and the dimer are the primary contributions to the absorption at 295 and 77 K, respectively, relative absorption intensities were used to determine values for equilibrium constants and ΔG at different temperatures (additional information in Section 3 of the Supporting Information). The temperature dependence of ΔG (Figure S3) was used to determine the dimerization enthalpy and

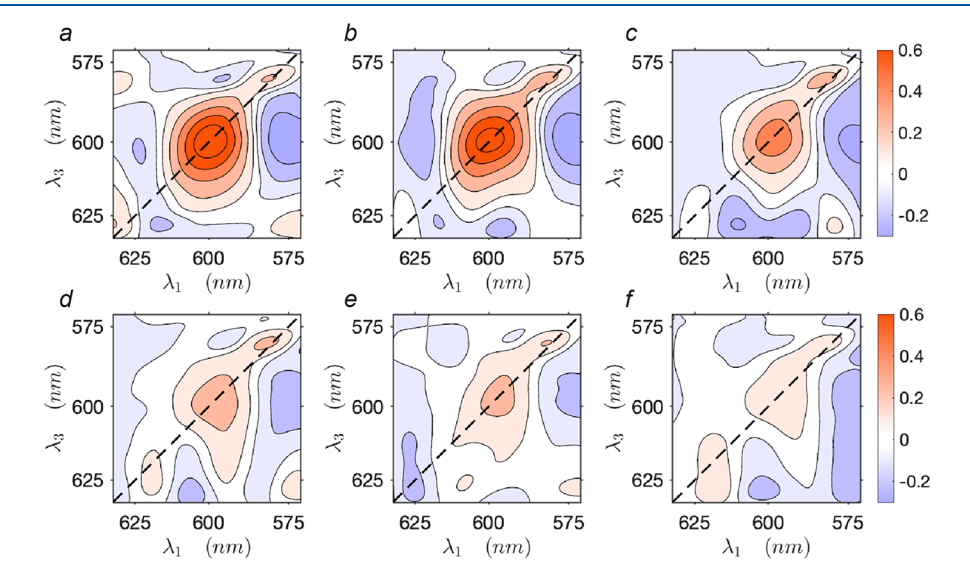


Figure 3. Representative absorptive 2DES surfaces for TD1–Cu at 295 K at various t_2 delay times: (a) 0.4, (b) 1.2, (c) 13, (d) 30, (e) 100, and (f) 400 ps.

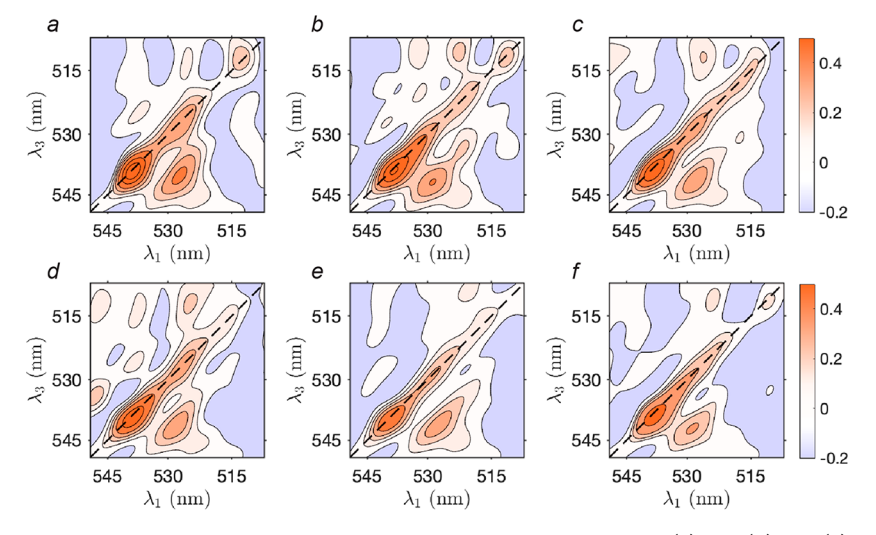


Figure 4. Representative absorptive 2DES surfaces for TD1–Cu at 77 K at various t_2 delay times: (a) 0.4, (b) 1.2, (c) 13, (d) 30, (e) 100, and (f) 400 ps.

entropy changes. The values obtained, $\Delta H = -4.07 \pm 0.08$ kcal/mol and $\Delta S = -21.9 \pm 0.3$ cal/(mol K), are consistent with previously published values. Both ΔH and ΔS are negative, indicating that dimerization is spontaneous at low temperatures. The temperature at which ΔG switches from positive to negative is approximately 185 K. This is consistent with our steady-state absorption spectra, which show a significant change between the 200 and 175 K traces.

Figure 3a-f present several representative 2DES spectra of TD1-Cu at room temperature. These spectra were acquired using a laser pulse centered at 600 nm, covering a spectral range of 570-633 nm. A brief description of the experimental setup is provided here (additional details can be found in Section 3 of the Supporting Information). The 2DES measurements were collected using a home-built femtosecond pump-probe geometry 2DES setup. A 1 kHz regenerativeamplifier laser system, Coherent (Libra), was used to power a home-built single-pass noncollinear optical parametric amplifier (NOPA). The NOPA output was compressed using a prism compression line and later split to generate pump and probe pulses. The pump pulse was passed through a pulse shaper, FASTLITE Dazzler, to provide a controllable variable time delay between two collinear pump pulses. This delay between the two pump pulses is called t_1 or the coherence time, and the delay between the pump pulses and the probe is called t_2 or the population time. The spot size of the pump and probe beams at the sample position was approximately 80 μ m. The NOPA output was centered at 600 and 529 nm for the room temperature (295 K) and 77 K measurements, respectively. The second harmonic generation signal generated with a BBO revealed a temporal width of sub-45 fs and sub-40 fs for the pulses used for the room temperature and 77 K measurements, respectively, which was complemented by polarization gated frequency resolved optical gating (PG-FROG) using a nonresonant sample (see Figures S4 and S5). After the sample position was determined, the probe was focused onto a spectrometer (SpectraPro HRS-300) and detected on a CCD (PIXIS 400, Princeton Instruments). The detection frequency axis collected using the CCD corresponds to the λ_3 axis in the 2DES plots; the λ_1 axis is generated from the Fourier transform of the delay between the pump pulses, t_1 . Each 2DES plot corresponds to a single point along the

population time, t_2 . Additional experimental details for the 2DES measurements can be found in the Supporting Information.

In Figure 3, the strong feature that appears on the diagonal at 600 nm in panel (a) is associated with a ground-state bleach (GSB) of the primary π -to- π * transition shown in the room temperature (295 K) absorption spectrum (Figure 2). A second ground-state bleach (GSB) feature associated with an electronic transition at 581 nm appears on the diagonal in Figure 3 (see also Figure S6), coinciding with the shoulder observed in the 295 K absorption spectrum. However, due to its proximity to the edge of the laser spectrum, the associated signal is weak. In Figure 3b-d, an excited-state absorption (ESA) feature is observed as an off-diagonal peak at $\lambda_1 = 606$ nm and $\lambda_3 = 625$ nm. Although this signal is extremely weak, we can assign it based on our previous work. It exhibits a blue-shift in its peak as the population time increases (Figure S7), which is consistent with our previous findings.

To determine the decay time scales associated with the diagonal 600 nm peak in Figure 3a–f, the associated region of the 2DES data was integrated (see also Figure S8) and plotted as a function of t_2 and fit to decaying exponentials. From these data, two time scales were recovered: 2.5 ± 0.4 and 13.8 ± 1.0 ps. These time scales are in agreement with our previously reported results for this system at room temperature, ¹⁴ with the shorter time scale corresponding to vibrational relaxation and the longer time scale to the lifetime of the excited state. Because of low signal, a reliable time scale could not be extracted from the ESA feature at $\lambda_1 = 606$ nm and $\lambda_3 = 625$ nm; however, that signal is also gone at long t_2 times.

The 2DES experiments at 77 K used a laser pulse with a central wavelength of 529 nm (Figure S2). This pulse is overlapped with the primary absorption feature in the 77 K spectrum. As the spectral bandwidth of this pulse did not span the entire transition, there is some shaping of the features in the 2DES spectrum due to a convolution of the absorption with the laser pulse. Figure 4 display representative 2DES surfaces at 77 K for various t_2 delays. The change in temperature from 295 to 77 K and the associated dimerization of TD1–Cu significantly changes the observed signal. At 295 K, the 2DES measurements are dominated by the GSB on the diagonal at 600 nm (Figure 3a–d), and all features disappear

on the order of tens of picoseconds. At 77 K, we observe two closely spaced narrow diagonal peaks at 528 and 539 nm (Figure 4a–f). These correspond to GSBs from two excitonic energy levels. A cross-peak also appears at λ_1 = 528 nm and λ_3 = 539 nm, associated with energy transfer between the higher to the lower state. The cross-peak appears due to electronic coupling in the dimer. All features observed in the 2DES spectra at 77 K persist to the maximum experimental delay of 400 ps, while at 295 K, the signal has fully decayed within the first 100 ps, highlighting the presence of much longer-lived excited state in the TD1–Cu dimer compared to its room temperature monomer counterpart.

The two diagonal peaks at 539 and 528 nm in the 77 K 2DES spectra arise from the GSB of two closely positioned electronic transitions originating from the triplet ground state of the dimer. Based on EPR measurements, 11 the ligand spin in the dimer is quenched due to strong antiferromagnetic coupling, while the spins on the Cu metal centers pair, resulting in a signal typical of a Cu(II) dimeric species with a spin triplet.¹¹ These GSB features are associated with the peak in the 77 K steady-state absorption spectrum (Figure 2) near 525 nm and a broad shoulder on the low-energy side. The signal corresponding to these GSBs persists throughout the entire experimental delay of 400 ps. Notably, the off-diagonal cross-peak between these two states is present from the beginning of the experiment, providing evidence of strong excitonic coupling between these states. This cross-peak also persists beyond the maximum experimental delay.

The decay time scales for the two diagonal peaks as well as the cross-peak below the diagonal in the 77 K 2DES data were determined by integrating the corresponding regions (Figure 5

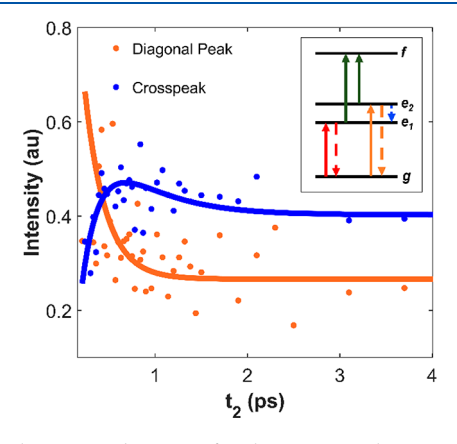


Figure 5. Short time dynamics for the 528 nm electronic transition and the cross-peak at $\lambda_1=528$ nm and $\lambda_3=539$ nm. The dots correspond to data points from integrated regions of the 2DES spectra at delay times, t_2 . The solid lines are fit with exponential terms reported in the main text. The inset presents the level structure for the dimer.

and Figures S9–S11) for all t_2 delay times and fitting those integrated traces with exponentials. The integrated trace of the GSB at 528 nm has a biexponential decay with time scales of 240 \pm 70 fs and a nanosecond time scale that persists beyond the maximum delay time of the 2DES experiment (400 ps). As the maximum experimental delay is significantly shorter than the lifetime of the signal, the associated nanosecond time scale cannot be reliably determined from the 2DES experiment. To determine this longer lifetime, a transient absorption measurement with a maximum delay of 1.4 ns was performed. The

recovery of the ground-state bleach was fit to exponential terms, recovering a long time scale of 1.0 ± 0.3 ns associated with the excited-state lifetime. The transient absorption data and associated fit can be found in Figure S12.

The lower energy state at 539 nm displays a biexponential decay profile with a fast decay component of 480 ± 60 fs, followed by a nanosecond time scale. Unlike the diagonal features, the cross-peak signal rises during the early population times with a time scale of 165 ± 70 fs. The higher energy diagonal peak has a corresponding but oppositely signed sub-250 fs time scale. These time scales are associated with an energy transfer process between the two states resulting from excitonic coupling. Following the rise in the signal from the fast energy transfer, the cross-peak then undergoes a biexponential decay with time scales of 460 ± 80 fs and a nanosecond time scale. The 460 and 480 fs time scales observed for the cross-peak and the diagonal peak at 539 nm, respectively, correspond to vibrational relaxation in the lower energy transition.

Both diagonal peaks as well as the cross-peak in the 77 K data persist beyond the maximum delay of the experiment. From the transient absorption measurement, the lifetime of the excited state at 77 K was found to be 1.0 \pm 0.3 ns. In contrast, at room temperature, the lifetime of the excited state is on the order of tens of picoseconds. The significantly longer excitedstate lifetime at low temperature means that the process facilitating fast (picosecond) excited-state relaxation in the monomer at 295 K is not available at 77 K due to a change in the electronic structure associated with dimerization. Fast excited-state decay in the monomer at 295 K is likely mediated through coupling to metal-centered states. Dimerization involves coupling between the spins localized on the copper metal centers and significantly modifies the electronic structure, as shown by the shift in the absorption spectra. This change in the electronic structure likely makes the 295 K deactivation pathway unfavorable, leading to longer-lived excited-state lifetimes.

The temperature-dependent change in the electronic structure arises from excitonic coupling in the dimer. At 77 K, the TD1-Cu dimer behaves like a model excitonic system. Upon dimerization, the resulting excitonic states, denoted as e_1 and e_2 in the inset in Figure 5, appear in the 77 K 2DES data at 539 and 528 nm, respectively. Up arrows signify transitions to higher energy electronic states, while down dashed arrows denote population relaxation to lower energy electronic states. The formation of an excitonic dimer at 77 K is supported by the observation of an energy transfer cross-peak. Based on the thermodynamic parameters (Supporting Information Section 2 and Figure S3) recovered from our absorption data, ΔG of dimerization is equal to zero at approximately 185 K. Considering the value of kT at that temperature, the coupling interaction driving dimerization is approximately 16 meV. In addition, the average energy of excitonic states is blue-shifted by approximately 250 meV with respect to the ground state in the dimeric form in comparison to the energy difference between the excited state and ground state of the monomer. This shift in energy is an order of magnitude greater than the coupling interaction, as expected for molecular dimers.^{24,25}

In conclusion, the temperature-dependent reversible spinmediated dimerization of TD1–Cu modifies the optical properties, leading to significant changes in the electronic structure and ultrafast dynamics. At room temperature, the triplet monomer form of TD1–Cu is a Cu(II)-bound radical whose excited state decays with a picosecond time scale. At 77 K, dimerization mediated by spin interactions between unpaired electrons on each of the monomers results in an excitonic system with a long excited-state lifetime. The unusual properties of TD1–Cu as a stable radical with two unpaired electrons results in spin-based temperature-switchable optical properties. These findings suggest that the TD1–Cu system may be useful as a spin- and temperature-controlled molecular switch with applications ranging from spin dynamics to redox chemistry and catalysis.

ASSOCIATED CONTENT

Supporting Information

The Supporting Information is available free of charge at https://pubs.acs.org/doi/10.1021/acs.jpclett.3c02726.

Details of the experimental methods, calculation of the thermodynamics parameters of dimerization, as well as supplemental spectroscopic data including steady-state absorption, pulse characterization, 2DES traces, transient absorption, and integrated data with corresponding fits (PDF)

AUTHOR INFORMATION

Corresponding Author

Vanessa Huxter — Department of Chemistry and Biochemistry, University of Arizona, Tucson, Arizona 85721, United States; Department of Physics, University of Arizona, Tucson, Arizona 85721, United States; orcid.org/0000-0001-9692-5312; Email: vhuxter@arizona.edu

Authors

Anshu Kumar – Department of Chemistry and Biochemistry, University of Arizona, Tucson, Arizona 85721, United States; Department of Physics, University of Arizona, Tucson, Arizona 85721, United States

Benjamin Thompson – Department of Chemistry and Biochemistry, University of Arizona, Tucson, Arizona 85721, United States; Department of Optical Sciences, University of Arizona, Tucson, Arizona 85721, United States

Ritika Gautam – Department of Chemistry and Biochemistry, University of Arizona, Tucson, Arizona 85721, United States Elisa Tomat – Department of Chemistry and Biochemistry,

University of Arizona, Tucson, Arizona 85721, United States; o orcid.org/0000-0002-7075-9501

Complete contact information is available at: https://pubs.acs.org/10.1021/acs.jpclett.3c02726

Notes

The authors declare no competing financial interest.

ACKNOWLEDGMENTS

V.M.H. gratefully acknowledges support from the donors of the American Chemical Society Petroleum Research Fund through grant no. 65536-ND6 and from the National Science Foundation through CAREER award grant no. 2236610. E.T. gratefully acknowledges support from the National Science Foundation through grant CHE-2203361. We thank Laura Sawyer for assistance with the transient absorption measurements.

REFERENCES

- (1) Himo, F.; Eriksson, L. A.; Maseras, F.; Siegbahn, P. E. M. Catalytic Mechanism of Galactose Oxidase: A Theoretical Study. *J. Am. Chem. Soc.* **2000**, *122* (33), 8031–8036.
- (2) Chaudhuri, P.; Wieghardt, K.; Weyhermüller, T.; Paine, T. K.; Mukherjee, S.; Mukherjee, C. Biomimetic Metal-Radical Reactivity: Aerial Oxidation of Alcohols, Amines, Aminophenols and Catechols Catalyzed by Transition Metal Complexes. *Biol. Chem.* **2005**, *386* (10), 1023–1033.
- (3) Capone, M.; Sirohiwal, A.; Aschi, M.; Pantazis, D. A.; Daidone, I. Alternative Fast and Slow Primary Charge-Separation Pathways in Photosystem II. *Angew. Chem., Int. Ed.* **2023**, 62 (16), No. e202216276.
- (4) Yoneda, Y.; Arsenault, E. A.; Yang, S., Jr.; Orcutt, K.; Iwai, M.; Fleming, G. R. The Initial Charge Separation Step in Oxygenic Photosynthesis. *Nature Comm* **2022**, *13* (1), 2275.
- (5) Saito, K.; Ishida, T.; Sugiura, M.; Kawakami, K.; Umena, Y.; Kamiya, N.; Shen, J.-R.; Ishikita, H. Distribution of the Cationic State over the Chlorophyll Pair of the Photosystem II Reaction Center. *J. Am. Chem. Soc.* **2011**, *133* (36), 14379–14388.
- (6) Narzi, D.; Bovi, D.; De Gaetano, P.; Guidoni, L. Dynamics of the Special Pair of Chlorophylls of Photosystem II. *J. Am. Chem. Soc.* **2016**, 138 (1), 257–264.
- (7) Twilton, J.; Le, C.; Zhang, P.; Shaw, M. H.; Evans, R. W.; MacMillan, D. W. C. The Merger of Transition Metal and Photocatalysis. *Nature Rev. Chem.* **2017**, *1* (7), 0052.
- (8) Huo, H.; Shen, X.; Wang, C.; Zhang, L.; Röse, P.; Chen, L.-A.; Harms, K.; Marsch, M.; Hilt, G.; Meggers, E. Asymmetric Photoredox Transition-Metal Catalysis Activated by Visible Light. *Nature* **2014**, *515* (7525), 100–103.
- (9) Hopkinson, M. N.; Sahoo, B.; Li, J.-L.; Glorius, F. Dual Catalysis Sees the Light: Combining Photoredox with Organo-, Acid, and Transition-Metal Catalysis. *Chem.—Eur. J.* **2014**, *20* (14), 3874–3886
- (10) Bahnmüller, S.; Plotzitzka, J.; Baabe, D.; Cordes, B.; Menzel, D.; Schartz, K.; Schweyen, P.; Wicht, R.; Bröring, M. Hexaethyltripyrrindione (H3Et6tpd): A Non-Innocent Ligand Forming Stable Radical Complexes with Divalent Transition-Metal Ions. *Eur. J. Inorg. Chem.* **2016**, 2016 (29), 4761–4768.
- (11) Gautam, R.; Astashkin, A. V.; Chang, T. M.; Shearer, J.; Tomat, E. Interactions of Metal-Based and Ligand-Based Electronic Spins in Neutral Tripyrrindione π Dimers. *Inorg. Chem.* **2017**, *56* (11), 6755–6762
- (12) Tomat, E. Coordination Chemistry of Linear Tripyrroles: Promises and Perils. *Comments on Inorganic Chemistry* **2016**, *36* (6), 327–342.
- (13) Tomat, E.; Curtis, C. J. Biopyrrin Pigments: From Heme Metabolites to Redox-Active Ligands and Luminescent Radicals. *Acc. Chem. Res.* **2021**, *54* (24), 4584–4594.
- (14) Cho, B.; Swain, A.; Gautam, R.; Tomat, E.; Huxter, V. M. Time-Resolved Dynamics of Stable Open- and Closed-Shell Neutral Radical and Oxidized Tripyrrindione Complexes. *Phys. Chem. Chem. Phys.* **2022**, 24 (26), 15718–15725.
- (15) Preuss, K. E. Pancake Bonds: π -Stacked Dimers of Organic and Light-Atom Radicals. *Polyhedron* **2014**, *79*, 1–15.
- (16) Kertesz, M. Pancake Bonding: An Unusual Pi-Stacking Interaction. *Chem.—Eur. J.* **2019**, 25 (2), 400–416.
- (17) Tomat, E.; Curtis, C. J.; Astashkin, A. V.; Conradie, J.; Ghosh, A. Multicenter Interactions and Ligand Field Effects in Platinum(II) Tripyrrindione Radicals. *Dalton Trans* **2023**, *52* (19), 6559–6568.
- (18) Habenšus, I.; Ghavam, A.; Curtis, C. J.; Astashkin, A. V.; Tomat, E. Primary Amines as Ligands and Linkers in Complexes of Tripyrrindione Radicals. *J. Porphyr. Phthalocyanines.* **2023**, 27, 1448–1456
- (19) Englman, R.; Jortner, J. The Energy Gap Law for Radiationless Transitions in Large Molecules. *Mol. Phys.* **1970**, *18* (2), 145–164.
- (20) Gouterman, M. Optical Spectra and Electronic Structure of Porphyrins and Related Rings. In *The Porphyrins*; Academic Press: New York, 1978; Vol. 3.

- (21) Straub, K. D.; Rentzepis, P. M.; Huppert, D. Picosecond Spectroscopy of Some Metalloporphyrins. *J. Photochem.* **1981**, *17* (2), 419–425.
- (22) Biswas, S.; Kim, J.; Zhang, X.; Scholes, G. D. Coherent Two-Dimensional and Broadband Electronic Spectroscopies. *Chem. Rev.* **2022**, *122* (3), 4257–4321.
- (23) Fuller, F. D.; Ogilvie, J. P. Experimental Implementations of Two-Dimensional Fourier Transform Electronic Spectroscopy. *Annu. Rev. Phys. Chem.* **2015**, *66* (1), *667*–690.
- (24) Van Amerongen, H.; Van Grondelle, R. *Photosynthetic Excitons*; World Scientific: Singapore, 2000.
- (25) Silinsh, E. A.; Capek, V. Organic Molecular Crystals: Interaction, Localization, and Transport Phenomena; AIP Press: New York, 1994.